Unraveling the Controls on Snow Disappearance in Montane Forests Using Multi-Site Lidar Observations

H. Safa[1,2], S. A. Krogh[1,3], J. Greenberg[1], T. S. Kostadinov[4] and A. A. Harpold[1,2,3]

[1]Department of Natural Resources and Environmental Science, University of Nevada, Reno, Nevada, USA.

[2]Graduate Program in Hydrologic Sciences, University of Nevada, Reno, Nevada, USA.

[3]Global Water Center, University of Nevada, Reno, Nevada, USA.

[4]Department of Liberal Studies, California State University San Marcos, California, USA

Corresponding author: Hamideh Safa (safa.hamideh@gmail.com; h.h.safa@nevada.unr.edu)

Key Points:

- Lidar datasets show the interacting role of topography and forest structure in differential snow retention in open vs. under canopy areas.
- Warm forests have increased interception and ablation from LWR, promoting snow retention in open areas, especially on south-facing slopes.
- Cold forest is influenced by SWR and wind sheltering, promoting snow retention under canopy, especially under lower vegetation density.

Abstract

Snow disappearance date (SDD) has a substantial impact on the ecohydrological dynamics of montane forests, by affecting soil moisture, ecosystem water availability, and fire risk. The forest canopy modulates SDD through competing processes, such as intercepting snowfall and enhancing longwave radiation (LWR) versus reducing near surface shortwave radiation (SWR) and wind speed. Limited ground-based observations of snow presence and absence have restricted our ability to unravel the dominant processes affecting SDD over mountains with complex forest structure. We apply a lidar-derived method to estimate fractional snow cover area (fSCA) at two relatively warm sites in the Sierra Nevada and two colder sites in the Rocky Mountain. Our analyses show that warm sites and lower elevations are characterized by higher LWR and canopy snow interception leading to less snow retention under dense forest canopy. In contrast, snow retention in colder forests can be longer in open or under canopy depending on interactions between vegetation structure and topography. These colder climates have greater under canopy snow retention on north-facing slopes and under low vegetation density areas, but greater snow retention in open areas at lower elevations and south-facing slopes. We develop a new conceptual model to incorporate the role of topography and vegetation structure into existing climate-based frameworks. The inferences into the interacting energy and mass controls, derived from our lidar datasets give opportunities to improve hydrological modeling and provide targeted forest management recommendations.

Plain Language Summary

Snow disappearance timing is a fundamental control on water availability for forest ecosystems and downstream water resources. In forested areas, trees intercept snowfall, shade the snowpack, and reduce wind speed. Warm trees also emit thermal (longwave) radiation that can melt the snowpack. Competition among these drivers controls variable snow disappearance timing in open areas versus under the tree canopy depending on climate, topography, and forest structure. In this paper we investigate how snowpack retention differs in the open versus under trees using novel snow-on and snow-off lidar observations. Our results show that snow disappears earlier under the canopy than in open areas in warmer, denser forests where the tree's thermal radiation and interception reduce under canopy snow retention. However, colder forests experience more

complicated tradeoffs between drivers of snowfall interception, shading, and wind sheltering. Snow retention in cold forests is greater under canopy areas on north-facing slopes, but switches to greater snow retention in open areas on south-facing slopes and at lower elevations. A unique lidar-derived dataset allows these process inferences, suggesting that tree canopy removal would benefit warm sites (especially south facing) for fire resilience and have the least benefit at cold sites (especially north facing).

1 Introduction

About 20% of global water supply is provided by melting ice and snow (Barnett et al., 2005), of which 40% falls in northern hemisphere forests (Stueve et al., 2011). Snowmelt timing and disappearance date have substantial impacts on the ecohydrological response of montane forests, by affecting soil moisture and deeper recharge (Bales et al., 2011; Conner et al., 2015; Flerchinger et al., 1992; Harpold et al., 2015b; Huntington and Niswonger, 2012; Pavlovskii et al., 2019), ecosystem water availability and streamflow timing (Harpold, 2016; Kormos et al., 2017, Stewart et al., 2004), growing season length (O'Leary et al., 2018; Harpold, 2016), spring phenology (O'Leary et al., 2018; Pederseng et al., 2018), soil greenhouse gas emission (Blankinship et al., 2018), and surface-atmosphere energy fluxes exchange (Knowles et al., 2014; Peichl et al., 2013; Slater et al., 2001). Since climate change portends shorter snow duration in montane forests (Bach et al., 2018; Cooper et al., 2016; Dibike et al., 2018; Li et al., 2017), improving predictions of snow retention is critical. However, processes and factors controlling the fate of seasonal snowpack are complex and strongly influenced by local climate, forest structure, and topography (Broxton et al., 2015; Dickerson-Lange et al., 2017; Lundquist et al., 2013; Tennant et al., 2017, Varhola et al., 2010). A lack of detailed snow observations across climate and topographic gradients in mountain forests has limited our ability to unravel the interacting processes that affect snow disappearance.

The influence of forest canopy on the duration of snowpack is complex, and results from tradeoffs between biophysical processes that reduce snow accumulation (e.g. snow interception and sublimation) versus processes that alter snowpack ablation (e.g. shading from shortwave radiation, (SWR), and sheltering from wind). Dense forests can intercept >50% of total snowfall in the winter (Ellis et al., 2011; Moeser et al., 2016; Roth and Nolin, 2017). Snow interception

and subsequent loss by sublimation and melt are the main factors causing longer snow duration in the open than under canopy locations in denser, warmer forests (Varhola et al., 2010) where interception efficiency is high (Dickerson-Lange et al., 2017; Storck et al., 2002). Decreased interception efficiency in windy cold forests (Roth and Nolin, 2017) and higher sublimation rates and blowing snow loss in cold, windy open locations cause snow to last longer in adjacent under canopy locations (Dickerson-Lange et al., 2017). Using a simple set of models, Lundquist et al. (2013) demonstrated a radiative paradox between LWR and SWR, specially at warmer sites where LWR is the primary radiative component of energy budget, controlling snow disappearance timing (Pomeroy et al., 2009; Lundquist et al., 2013). The increased role of LWR at the warm sites caused snow to disappear one to two weeks earlier under tree canopies compared to adjacent open areas (Lundquist et al., 2013), in spite of the canopy shading snow from SWR. High emissivity of warm trees enhances LWR emission toward the snowpack that frequently exceeds atmospheric LWR by 150% (Todt et al., 2018; Webster et al., 2016a; Perrot et al., 2014). Net LWR is typically positive under 100% canopy cover and can affect the energy budget of snowpack within one-half nearby tree heights (Musselman et al., 2017), whereas it is typically negative in the open locations (Lundquist et al., 2013). Incoming SWR is modulated by solar zenith angle, cloudiness and aerosol concentrations in the atmosphere (Musselman et al., 2015) and it can be reduced by tall and dense canopy cover and terrain shading at the snow surface (Jonas and Essery, 2011; Malle et al., 2019; Webster et al., 2016b). In late winter and spring, when the solar zenith angle decreases (i.e. the Sun is higher in the sky), SWR shading can delay snowmelt under forest canopies, especially in cold climates (Strasser et al., 2011; Lundquist et al., 2013). Besides the radiative influence of trees on the snowpack energy budget, sensible and latent heat gradient between trees and the snowpack are not negligible and can substantially contribute to the snowpack energy budget specifically at cold windy sites (Harder et al., 2019; Webster et al., 2016b; Todt et al., 2018). The tradeoffs of these processes on the differential timing of snow disappearance in open and under canopy areas has primarily been investigated at point scale (Lundquist et al., 2013; Dickerson-Lange et al., 2017) and not considered forest structure.

The interactions between forest structure and topography (e.g. elevation, aspect, and slope) differentially alters the energy and mass balance of open and under canopy snowpack in ways

that are challenging to observe and predict across varying climates. The current paradigm for predicting differential snow disappearance under canopy and in open areas shows that locations with December-February (DJF) mean air temperature above -1°C have earlier snow disappearance under canopy areas (Lundquist et al., 2013), whereas sites with DJF mean air temperatures below that threshold exhibit earlier snow disappearance in open areas. This paradigm was developed from plot-scale observations and has not been applied across gradients in elevation or slope-aspect typical of larger montane, forested areas. For example, elevation is often the primary control on snow duration, as higher elevations have more precipitation and lower temperatures, causing greater snow to rain ratios, and higher cold content of the snowpack (Lundquist et al., 2013; Molotch and Meromy, 2014; Roth and Nolin, 2017). Similarly, warmer northern-hemisphere areas have longer snow retention on northern slopes (Lopez-Moreno et al., 2014; Maxwell et al., 2019; Seyednasrollah et al., 2013) due to differential partitioning of incoming SWR and LWR. Heterogeneous forest canopy structure (e.g. height and leaf area) and differences in inter-canopy gaps are important factors controlling fine-scale snow retention (Jonas and Essery, 2011; Webster et al., 2016b). The first-order effects of topography and forest structure on snow retention (Malle et al., 2019; Webster et al., 2016b), suggest that a more sophisticated prediction tool beyond air temperature may be necessary to provide information on snow disappearance in montane forests.

New remote sensing tools, like airborne-based Light Detection and Ranging (lidar), could revolutionize our understanding of snow disappearance timing in forests with complex terrain, where only limited plot-scale field observations have been available to date. Ground-based observation such as snow courses, temperature loggers, and time-lapse cameras (Dickerson-Lange et al., 2015b; Raleigh et al., 2013) can be used to estimate snow disappearance date (SDD, defined as the first date when snow disappears after peak SWE). Dickerson-Lange et al. (2015a; 2017) collected spatially distributed snow data and show that cameras can detect snow presence or absence with higher spatial resolution than ultrasonic snow depth sensors, however their installation over larger extents is challenging. Other ground-based methods that are capable of measuring snow disappearance over larger extents, like distributed temperature sensing (DTS) (Tyler et al., 2009), are typically too costly to maintain, automate, and operate over large domains (Dickerson-Lange et al., 2015b; Fujihara et al., 2017). One of the major limitations of

passive (i.e. optical) remote sensing techniques is their inability to detect under canopy snowpack presence/absence due to occlusion by the canopy (Raleigh et al., 2013; Coons et al., 2014). Most of remote sensing prediction estimate fractional snow cover area, fSCA, or the percentage of a given area covered by snow, but assume that open and under canopy fSCA are identical (Molotch and Margulis, 2008; Raleigh et al., 2013). A new method based on "snow on" and "snow off" lidar datasets showed that under canopy fSCA was typically much less than open fSCA in a northern Sierra Nevada site, but that relationship varied with topography (Kostadinov et al., 2019). Snow disappearance and fSCA are inter-related, as fSCA decreases snow must be disappearing from the landscape; thus, lidar-based fSCA estimates can potentially elucidate differential snow retention in open versus under canopy locations during 'snap shot' lidar collections (Kostadinov et al., 2019). Because lidar can also map topography and vegetation structure, these methods are ideally suited for understanding the interactions of forest structure and topography in controlling snow retention in montane forests (Deems et al., 2013; Revuelto et al., 2015; Harpold et al., 2015a; Tennant et al., 2017; Kostadinov et al., 2019).

In this paper we aim to unravel how winter climate interacts with topography and vegetation structure to alter snow disappearance in open versus under canopy locations. We leverage existing snow-on and snow-off lidar observations at two relatively warm sites in the Sierra Nevada (Sagehen Creek Watershed, California and Kings River Experimental Watersheds, California) and two colder sites in the Rocky Mountains (Boulder Creek, Colorado and Jemez River Basin, New Mexico) to map fSCA over large spatial extents using the technique proposed by Kostadinov et al. (2019). This analysis allows us to answer three questions:

1) How do open and under canopy fSCA and snow disappearance date (SDD) vary based on slope/aspect and elevation at sites with different climate?

2) Does vegetation structure have greater impact on under canopy fSCA and SDD in some climates and/or topographic conditions than in others?

3) What are the inferred energy and mass balance drivers causing differences in fSCA and SDD across open versus under canopy areas in warmer and colder climates?

Our results provide insights into the role that topography and forest structure play in modulating

snow retention across a climatic gradient of montane forests.

2 Study Sites and Data

We chose four sites, two in the USA Rocky Mountains: Boulder Creek, Colorado, CO and Jemez River Basin, NM, and two in the Sierra Nevada: Sagehen Creek Watershed, CA, Kings River Experimental Watersheds, CA (Figure 1). These sites represent strong climate and vegetation gradients, have snow-on and snow-off lidar datasets and detailed point observations of snow depths for multiple years, including years that overlap with the lidar flights acquisition. Site characteristics are shown in Table 1, including average watershed slope and aspect, field observation and lidar data acquisition years, vegetation type and average forest height (Harpold et al., 2015b; Tennant et al., 2017; O'Geen et al., 2018; Kostadinov et al., 2019).

2.1 Boulder Creek, CO (Boulder)

Boulder Creek, hereafter referred as Boulder, is located 35 km west of the city of Boulder, Colorado, USA, and is part of the U.S. National Science Foundation network of Critical Zone Observatories (CZOs). Boulder is the coldest of the four study sites with an average annual air temperature of 10°C (Harpold et al., 2015) and mean winter (DJF) air temperature of −5.4°C (Table 1). The mean annual ratio of incoming shortwave radiation to incoming net radiation is 0.43 (SWR↓:NetR↓= 149.6 /(149.6+199.9), Table 1, Tennant et al., 2017). The average wind speed in winter is 6.5 m/s and the total annual precipitation is 1300 mm, of which 80% is snow (Harpold et al., 2015a). The site is equipped with ultrasonic snow depth sensors in the open and under canopy sites; snow depth data were recorded from 2007 to 2011. Snow depth in-situ data is used to track the snow disappearance date for five continuous years. In this site snow depth has a positive relationship with elevation with a rate of 0.73 ± 0.2 cm per 100 m increase in elevation (Tennant et al., 2017). A Snow Telemetry (SNOTEL) site is located within 1 km of the snow depth sensors. The dominant vegetation is subalpine fir (*Abies lasiocarpa*), Engelman spruce (*Picea engelmannii*) and lodgepole pine (*Pinus contorta*). The snow-off lidar survey for Boulder was conducted in a 600 km^2 area within the Boulder Creek Watershed in August 2010. The lidar snow-on surveys were acquired in May 5, 9, 20, and 21, 2010, and were combined together for the same area as the snow-off lidar survey (Table 2). The lidar products are available at Open

Topography (http://opentopo.sdsc.edu/datasets) in the NAD83 datum and are composed of 1-m Digital Terrain Models, and LAS-formatted point cloud tiles with an average point density of 10 points/m^2.

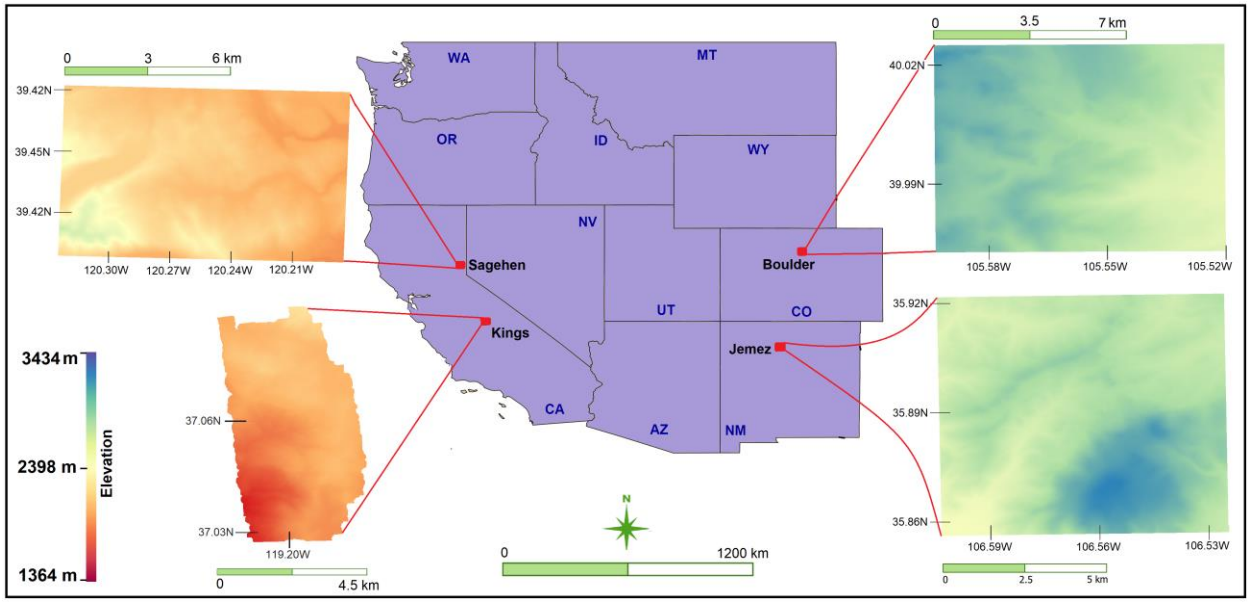

Figure 1: Location, lidar-based terrain elevation and the extent of processed lidar data at the four study sites: Sagehen Creek Watershed, CA, Kings River Experimental Watersheds, CA, Boulder Creek, CO and Jemez River Basin, NM.

2.2 Jemez River Basin, NM (Jemez)

The Jemez River Basin, hereafter referred as Jemez, is a CZO site at the southern end of the Rocky Mountains in northern New Mexico, USA. The average winter temperature and wind speed are −3.3°C and 3.9 m/s, respectively. The ratio of SWR↓:NetR↓ is 0.44, which is the highest among our sites (Tennant et al., 2017). The total annual precipitation in the basin is around 1980 mm of which 66% is snowfall. In-situ data measurement includes ultrasonic snow depth sensors under canopy and in the open, which are used to track the snow disappearance date. The snow depth observations were recorded from 2005 to 2011 (excluding 2007) at an elevation of 3060 MASL at Jemez (Tennant et al., 2017). Forest covers 33% of the basin with various types of conifers, including Douglas fir (*Pseudotsuga menziesii*), white fir (*Abies concolor*), blue spruce (*Picea pungens*), limber pine (*Pinus flexilis*) and ponderosa pine (*Pinus*

ponderosa) (Harpold et al., 2015b). High-resolution snow-off lidar surveys were carried out in June and July 2010 by the National Center for Airborne Laser Mapping (NCALM), covering an area of 722 km^2 in northern New Mexico. Lidar products have an average cloud point density of 9.08 points/m^2. The point cloud data are provided in LAS format in the NAD83 datum at open Topography (http://opentopo.sdsc.edu/datasets); 1-m Digital Surface Model (DSM) and 1-m hill shade dataset derived from DEM are also provided. The Jemez snow-on lidar dataset was collected in March and April 2010 (Table 2).

2.3 Kings River Experimental Watershed, CA (Kings)

Kings River Experimental Watersheds, hereafter referred as Kings, is mostly located within the Providence Creek in the west slope of the southern Sierra Nevada in California, USA. Kings has an average elevation of 1846 MASL. Annual precipitation in the watershed is about 2000 mm, of which 75%-90% falls as snow. We use ultrasonic snow depth sensors at Kings between 2010 and 2012 to determine the presence or absence of snow under canopy and in the open. Average winter wind speed and SWR↓:NetR↓ in the watershed are about 1.6 m/s and 0.36, respectively (Tennant et al., 2017). Average annual and winter (DJF) air temperatures are 8°C and 2.2°C, respectively (O'Geen et al., 2018). This domain is mostly covered by mixed-coniferous forest (60%), consisting of white fir (*Abies concolor*), ponderosa pine (*Pinus ponderosa*), Jeffrey pine (*Pinus jeffreyi)*, California black oak (*Quercus kelloggii*), sugar pine (*Pinus lambertiana Douglas*), and incense cedar (*Calocedrus decurrens*) (O'Geen et al., 2018). Kings lidar flights were part of a larger Southern Sierra CZO effort acquired in 2010, comprising of two flights, a snow-on flight in March and a snow-off one in August. The lidar product projection is UTM Zone 11 N with datum NAD83 (Table 2). This dataset includes a 1-m digital surface model (DSM) and a LAS-formatted cloud point with an average point density of 11.6 point/m^2 in 1 km by 1 km tiles.

237 Table 1: Characteristics of the study sites

Characteristics	Kings River Experimental Watershed, CA	Sagehen Creek Watershed, CA	Jemez River Basin, NM	Boulder Creek, CO
Latitude (at the center of lidar dataset domain)	37°5′N	39°25′53″N	35°53’18″N	40°0’53″N
Longitude (at the center of lidar dataset domain)	119°28’W	120°14′23″W	106°31’55″W	105°16’14″W
Mean elevation (MASL – in lidar dataset domain)	1846	2200	2702	3109
Slope (degrees)	~ 22	15.8	7.0 ± 3.7	7.3 ± 3.5
Aspect (from N)	~ 312	~159	164 ± 105	94 ± 61
Average winter[1] temperature (°C)[2]	2.2	~ -1	−3.3 ± 0.3	−5.4 ± 2.6
Total winter Precipitation (mm)[2]	2000	590	580	1300
Average daily winter incoming SWR (W/m^2)[2]	209.1	127.97	150.6	149.6
Average daily winter incoming LWR (W/m^2)[2]	251.3	254.4	201.6	199.9
Vegetation type	Mixed conifer	Mixed conifer	Mixed conifer	Mixed conifer
Average forest height (m)[2]	13.3	15	7.7 ± 4.4	7.2 ± 2.8
Average vegetation density (in areas with slope < 30°)[2]	0.59	0.3	0.4	0.47
Temperature lapse rate equation[3]	– 0.003 × elevation + 7.29	T_{Mar} = – 0.001 × elevation + 2.79 T_{Apr} = – 0.001 × elevation + 2.05 T_{May} = – 0.002 × elevation + 5.25	– 0.005 × elevation + 8.67	– 0.007 × elevation + 17.82
Precipitation lapse rate equation[3]	0.06 × elevation - 13.978	0.08 × elevation - 130.65	0.006 × elevation + 15.52	0.03 × elevation - 68.98
Source of climate data used	https://www.fs.fed.us/psw/topics/water/kingsriver/data.shtml https://www.wcc.nrcs.usda.gov/snow/snotel-data.html	https://www.nrcs.usda.gov/wps/portal/wcc/home/snowClimateMonitoring/	https://criticalzone.org/catalina-jemez/infrastructure/field-area/jemez-river-basin/ https://www.wcc.nrcs.usda.gov/snow/snotel-data.html	https://www.nrcs.usda.gov/wps/portal/wcc/home/snowClimateMonitoring/ https://wcc.sc.egov.usda.gov/nwcc/site?sitenum=663

238 [1] Averaged over December, January, and February.
239 [2] Calculated over the entire domain.
240 [3] details given in section 3.

241 Table 2: Lidar dataset properties for each study sites

Properties	Kings River Experimental Watershed, CA	Sagehen Creek Watershed, CA[1]	Jemez River Basin, NM	Boulder Creek, CO
Organization acquired the flight	National Center for Airborne Laser Mapping, funded by National Science Foundation And Southern Sierra Critical Zone Observatory	National Center for Airborne Laser Mapping, Funded by USDA Forest Service and U.S. Geological Survey	National Center for Airborne Laser Mapping, Jemez River Basin and Santa Catalina Mountains Critical Zone Observatory, University of California, Merced, Funded by National Science Foundation	Boulder Creek CZO and the National Center for Airborne Laser Mapping (NCALM), funded by the National Science Foundation (NSF)
Sensor	Optech GEMINI Airborne Laser Terrain Mapper mounted in either a twin-engine Cessna Skymaster (N337P) or Piper Twin PA-31 Chieftain	Optech Gemini Airborne Laser Terrain Mapper (ALTM) mounted in a twin-engine Piper Navajo PA-31	Optech GEMINI Airborne Laser Terrain Mapper mounted in either a twin-engine Cessna Skymaster (N337P) or Piper Twin PA-31 Chieftain	Optech Gemini Airborne Laser Terrain Mapper (ALTM) mounted in a Piper Twin PA-31 Chieftain
Flight altitude	600 m	600 m	600m	600m
Laser wavelength	1047 nm	1047 nm	1047 nm	1047 nm
Average point density	11.65 points/m^2	8.93 points/m^2	9.08 points/m^2	8 - 10 points/m^2
Swath overlap	50%	>50%	50%	50%
Vertical accuracy	5 - 30 cm; 1 sigma	5 - 30 cm; 1 sigma	5 - 30 cm; 1 sigma	5 - 30 cm; 1 sigma
Horizontal accuracy	1/5,500 x altitude (m AGL); 1 sigma	1/5,500 x altitude (m AGL); 1 sigma	1/5,500 x altitude (m AGL); 1 sigma	1/5,500 x altitude (m AGL); 1 sigma
Vertical datum	NAVD88 (GEOID 12A)	NAVD88 (GEOID 12A)	NAVD88 (GEOID 12A)	NAVD88 (GEOID 12A)
Horizontal datum	UTM Zone 11N NAD83	UTM Zone 10N NAD83 (2011)	UTM Zone 13N NAD83	UTM Zone 13N NAD83
Time of Acquisition Snow-off	August 2010	August 2014	June and July 2010	August 2010,
Time of Acquisition snow-on	March, 2010	March, April, and May 2016	March and April 2010	May 5, 9, 20, and 21, 2010

242 [1] information provided here is same for all Sagehen flights

243

2.4 Sagehen Creek Watershed, CA (Sagehen)

Sagehen Creek Watershed, hereafter referred as Sagehen, has a drainage area of 28 km^2 and is located in the northern Sierra Nevada, California. The average elevation is 2200 MASL ranging between 1800 and 2700 MASL. Average winter temperature is approximately -1.2 °C and the mean annual precipitation is 1215 mm, of which 70% is snowfall (WRCC, 2020). Sagehen is a forested montane watershed covered by mixed conifers including White Fir (*Abies concolor*), Red Fir (*A. magnifica*), Lodgepole Pine (*Pinus contorta*), Jeffrey Pine (*P. jeffreyi*), Sugar Pine (*P. lambertiana*), Western White Pine (*P. monticola*), and Ponderosa Pine (*P. ponderosa*) (Godsey and Kirchner, 2014; Li and Nieber, 2017). The snow-off surveys were conducted by NCALM (USFS, 2015) in the summer of 2014, as part of the USFS Tahoe National Forest lidar collection (Table 2). Snow-on datasets were acquired in March 26, April 17, and May 18, 2016, by the NASA Airborne Snow Observatory (ASO) (Painter et al., 2016). In-situ distributed temperature sensor (DTS) is used as ground-based observation data to assess the presence or absence of snow under canopy and in the open. DTS records near-continuous temperatures along a fiber optic cable by applying a Raman spectrum scattering and time-domain reflectometry techniques (Tyler et al. 2009). The DTS instrumentation in Sagehen recorded ground temperature every 30 min between March 10 and May 18, 2016, every 0.25 m along a 1500-m stretch of fiber optic cable. At each 0.25-m point along the DTS cable, we assume snow is on the ground if the daily air temperature is between -1 and 1°C and the daily standard deviation of observed temperatures is less than 0.35 °C. The cable was georeferenced to the UTM WGS84 coordinate system and converted to NAD83 to match the lidar dataset (Kostadinov et al. 2019). More details on the DTS measurements and data processing can be found in Kostadinov et al. (2019).

3 Materials and Methods

3.1 Vegetation and Snow Presence/Absence Classification

Vegetation and snow presence classifications introduced by Kostadinov et al. (2019) are used to estimate under canopy and open fSCA at all sites. Point-cloud lidar data is aggregated to a raster resolution of 1-m grid cells to classify vegetation structure and snow presence/absence within

each study site. To enhance the accuracy of the vegetation and snow presence classification, slopes greater than 30° are excluded from the analysis, as the uncertainty in elevation estimates increases significantly (Kostadinov et al. 2019). At each site, a small section of a road that is maintained snow-free, is selected and used to compare snow-on and snow-off flights to eliminate any potential vertical bias between the snow-on lidar return elevations and the snow-off digital terrain model (DTM). The comparisons show that snow-on elevation returns in each grid cell over roads are 0.28 m, 0.08 m, and 0.03 m higher than snow-off returns for Kings, Jemez and Boulder respectively. Kostadinov et al. (2019) made the same analysis for three flights over Sagehen and concluded three mean vertical biases of 0.23 m, 0.26 m, and 0.38 m for the March 26, April 17 and May 18, 2016, respectively. These biases are subtracted from all snow-on return elevations (see Kostadinov et al. (2019) for details).

Vegetation presence is classified using the snow-off lidar. A 1-m grid cell is defined as tree-covered if there is any lidar return above 2 m in the grid. If the tree-covered grids have any return between 0.15 and 2 m, those grids are classified as tree-covered with low branches. The latter grid cells are removed from the analysis because low branches can be confused with the snow surface during the snow-on flights (Kostadinov et al. 2019). Grid cells with all returns below 0.15 m are classified as open sites. To determine snow presence/absence under the canopy and in the open, the snow-on flights' classification is informed by the vegetation classification. If a tree-covered grid cell (low branches grid cells excluded) has returns with elevation between 0.15 m and 5 m, it is classified as snow-covered (presence). If the return's elevation is between -0.3 m (i.e. below the 1-m mean grid cell elevation) and 0.15 m, the grid cell is classified as snow-free. Same approach is used to classify open grid cells as snow-covered. More details on the classification approach are presented by Kostadinov et al. (2019). Under canopy fSCA is calculated by dividing the number of vegetated grid cells classified as snow-covered by the total number of tree-covered grid cells within the entire domain of a site. Whereas fSCA in the open is calculated by dividing the number of 'open' (i.e. non-vegetated) grid cells classified as snow-covered by the total number of 'open' grid cells in the entire lidar coverage domain. fSCA in open and under canopy sites are then computed over different sub-domains with different elevation and vegetation characteristics (see section 4.2).

Vegetation density is calculated by dividing the number of lidar returns that hit the canopy (i.e.

height >2 m) by the number of total returns in each 1-m grid cell (Broxton et al., 2015). If the vegetation density is below 0.4 the pixel is classified as a low vegetation density (lowVD) and greater than 0.6 is classified as high density (highVD). We exclude grid cells with moderate vegetation density from 0.4 - 0.6 from the analysis, because our goal is to investigate and differentiate the effect of low and high vegetation density on SDD.

3.2 Topographic Classification

To investigate the impact of aspect and slope on open and under canopy fSCA and snow disappearance date (SDD), a northness index (Amatull et al., 2018) is calculated from the DTM for each site, so that:

$$\text{Northness} = \cos(\text{aspect}) \times \sin(\text{slope})$$

where slope and aspect are given in radians, and aspect is measured clockwise from true north. Northness is +1 on north-facing terrain with steep slopes of 90°, and −1 on south-facing terrain with slopes of 90°. Northness is 0 for flat terrain. Grid cells are classified as "exposed" if Northness < -0.1, "flat" if -0.1 < Northness < 0.1, and "sheltered" if Northness > 0.1. In the extratropical Northern Hemisphere, terrain with Northness < -0.1 is exposed to more solar radiation during afternoon heat for locations with the same latitude.

Each domain is binned into ten elevation bands to study the effect of elevation on open and under canopy fSCA. These bands cover ranges of 2820-3050 MASL, 2800-3130 MASL, 2100-2400 MASL and 1600-1850 MASL for Boulder, Jemez, Sagehen and Kings, respectively (Figure 1). Relationships between elevation and air temperature and precipitation (i.e. lapse rates) for each site-flight are developed using observed (mean daily) air temperature and precipitation from local weather stations (Table 1) from December 1st to the date of the flights (we did not consider cold air drainage or temperature inversion in our analysis). These relationships are used to estimate mean air temperature at each sites' elevation bands. Classified grid cells within each site and elevation band are then divided into 100 areas and from each sub-division area a random sample (sample size =100 grid cells) is choses. We repeat this random sub-sampling for 100 times, and average them. The under canopy and open fSCA is calculated for each averaged sub-sample within each sub-division. Then, the Wilcoxon signed-rank test at a 5% level of

significance is conducted to examine whether under canopy and open fSCA are statistically different using the 100-samples per each subdivision in each elevation band. The p-values from the 100-samples are averaged at each subdivision and elevation band to estimate if the under canopy and open fSCA are statistically different.

3.3. Random Forest Modeling to Analyze Vegetation and Climate Impacts on FSCA

A machine learning approach based on a regression type of random forest model (RFM) is used to examine the importance of radiative and mass fluxes in controlling under canopy vs. open fSCA. RFM utilizes an ensemble of regression trees to build a predictive model based on a series of predictors and a response variable (here, $fSCA_{open} - fSCA_{underCanopy}$). RFM is also used to rank predictors' importance. Six RFMs are developed for each lidar flight (three for Sagehen and one for each remaining domain) to predict the difference between $fSCA_{open}$ and $fSCA_{underCanopy}$ at 100-m resolution. Included predictor variables are vegetation density, incoming SWR and LWR, precipitation and mean winter air temperature. We did not include topographic variables, such as elevation and aspect/slope, because they are already captured in air temperature and SWR predictor variables. The average air temperature and precipitation of each 1-m grid cell are calculated using lapse rate equations described in the previous section and shown in Table 1. Then, averaged precipitation and winter air temperature are computed in the scale of 100 m grid cells for the RFMs. Hourly incoming SWR and LWR at the top of the canopy are calculated using the pre-processing toolbox of the Snow Physics and Lidar Mapping model (SnowPALM; Broxton et al., 2015) at 1-m spatial resolution. SnowPALM is forced with hourly incoming SWR and LWR from phase-2 of the National American Land Data Assimilation System (NLDAS-2; Xia et al., 2012). SWR is spatially distributed using the potential surface SWR as estimated by the method from Kumar et al. (1997) and corrected for terrain shadowing. Incoming SWR and LWR are averaged to daily 100-m grid cells from December 1st to the date of each flight. The number of trees in our RFM is 200, as higher number of trees does not change the accuracy of results. We randomly select 70% of our data to train the model and the remaining 30% data for verification. To lower bias in selection of the training and verification data, we apply K-fold (here 10-fold) cross-validation procedure. This technique splits the dataset into 10 random groups that train and test the model independently. K-fold is one of the resampling approaches

which is commonly used to avoid RFM overfitting (Cawley and Talbot, 2010). The mean absolute error (MAE) metric is used to evaluate the accuracy of the RFM's predictions:

$$\text{MAE} = \sqrt{\frac{\sum_{i=0}^{n}|x_i - y_i|}{n}}$$

where x_i is the observed [$fSCA_{open}$ – $fSCA_{underCanopy}$], y_i is the modeled [$fSCA_{open}$ – $fSCA_{underCanopy}$] and n is the number of the 100-m grid cells.

To explore the importance of our predictors across a range of fSCA, grid cells are classified into four bins for each flight, fSCA<0.3, 0.3<=fSCA<0.55, 0.55<=fSCA<0.8 and 0.8<=fSCA to have a roughly same number of grid cells in each bin, and simultaneously exclude grid cells with fSCA>0.99 and fSCA<0.01. This classification allows a better comparison between predictor variables among sites with highly variable snow disappearance date.

4 Results

4.1 Observed differences in open and under canopy snow disappearance

We use ultrasonic snow depths observation at Boulder, Jemez and Kings, and DTS data at Sagehen to determine snow disappearance date (SDD, first date when snow disappears after peak SWE) in open and under canopy sites. Snow generally lasts longer under canopy at the colder Jemez and Boulder sites (T_{DJF} < -1°C), but not in the warm and dry years of 2006 at Jemez, and 2007 and 2010 at Boulder. Mean SDD, including both open and under canopy, is approximately two months later at Boulder than at Jemez (Figure 2). The average standard deviation of snow disappearance across the sensor locations at Jemez is relatively small in the open and under canopy (1.5 and 5.0 days, respectively). One mean standard deviation of SDD at Boulder is 7.8 days under canopy sites and 3.8 days in the open sites. In contrast, snow lasts 5.0 and 7.3 days longer on average in the open at the warmer Sagehen and Kings sites (T_{DJF} > -1°C), respectively. SDD happens about 41 days earlier in Sagehen than Kings. The mean standard deviation of SDD is larger for open and under canopy in Sagehen (15.2 and 18.1 days respectively) than Kings (5.8 and 10.6 days, respectively) and the colder sites (note that we consider each DTS point as a single sensor, and calculate standard deviation of SDD for a sample of 1500 DTS points).

Figure 2: SDD (snow disappearance day) under canopy and in the open sites in different years at Sagehen (a), Kings (b), Jemez (c) and Boulder (d) sites. We used snow depth observations from the ultrasonic sensors at Boulder, Jemez and Kings, and DTS data at Sagehen to determine SDD.

Since snow must be disappearing off the landscape for fSCA to decline, decreased fSCA on a given date is related to earlier SDD, i.e. if fSCA is lower, this implies SDD must be earlier in the season. We explore the relationship between SDD and fSCA at Sagehen to help interpret later fSCA-based analyses. The relationship between fSCA and SDD is estimated by calculating fSCA and SDD every 10 m of the DTS cable for every day in the melting season. We assume every 10 m of DTS cable as a grid cell, and snow presence/absence data is sampled every 25 cm, hence there are 40 values of snow presence (1) or absence (0). For instance, if the number of "1" values equal 20, then fSCA is 20/40 = 0.5. Figure 3 depicts fSCA-SDD relationship at Sagehen

on the day of lidar flights in April 17 (a) and the slopes of daily sigmoid fSCA-SDD relationships for fSCA between 0.2 to 0.8 from April 2 to April 28, 2016 in Sagehen. A fitted sigmoidal relationship between fSCA and SDD has the highest correlation with observed data (R^2=0.76) on April 17, when a decline of fSCA from 0.8 to 0.2 is equivalent to 20±3.1 days change in SDD. The correlation of fSCA-SDD relationships is much weaker in March and May 2016. This relationship is from a single site within Sagehen with low variation in topography (Kostadinov et al. 2019), thus, we expect this to be a conservative estimate for the sensitivity (e.g. slope) of SDD to fSCA across more extreme snow or energy gradients.

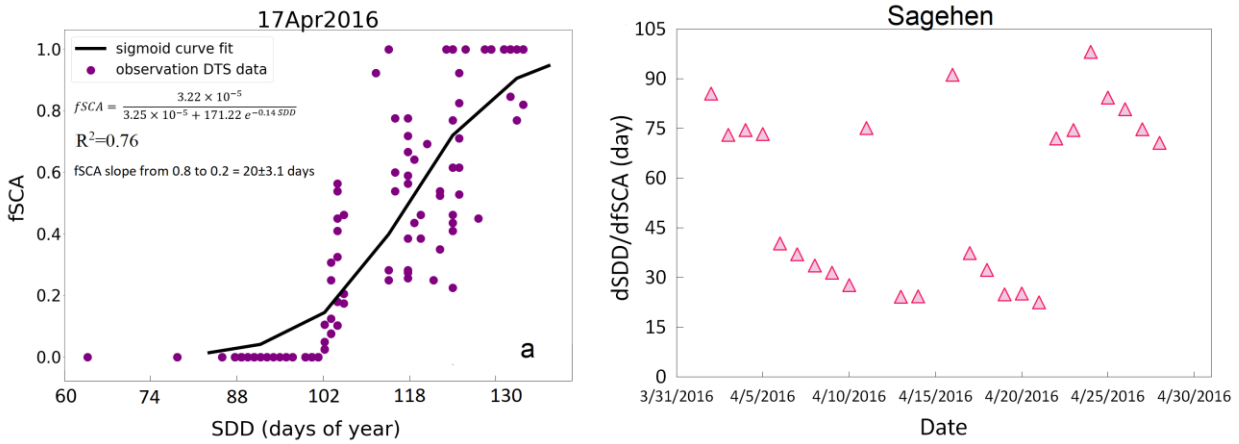

Figure 3: Relationship between fSCA and SDD in a small site within Sagehen on April 17, 2016 (a) and the slopes of daily sigmoid fSCA-SDD relationships for fSCA between 0.2 and 0.8 from April 2 to April 28, 2016 (b).

4.2 Lidar-derived relationships of snow retention differences and topography

Binary snow presence or absence, calculated at 1m resolution with lidar observations, is used to determine under canopy and open area fSCA in each T_{DJF} band for the six lidar flights (Figure 4): Boulder in May 2010, Jemez in April 2010, Kings in March 2010, and Sagehen in March 26, April 17 and May 18, 2016. In general, fSCA is higher when T_{DJF} is colder (i.e. elevation increases) at all sites. fSCA under canopy is significantly higher than that in the open at the coldest Boulder site in T_{DJF} bands < -7 °C (Figure 4-f), though this difference is insignificant at the coldest T_{DJF} band. At Jemez, there are not large differences between under canopy and open fSCA in T_{DJF} bands <-5°C, primarily because fSCA is close to 100%. Conversely, fSCA in the

418 open is significantly higher than under the canopy (Figure 4-e) for T_{DJF} bands > -5.5 °C at
419 Jemez. At the warmer sites of Sagehen and Kings, fSCA is generally larger in the open relative
420 to under canopy. However, in warmer T_{DJF} bands of Kings (T_{DJF} > +2°C) where fSCA is <40%,
421 under canopy is higher than open fSCA (Figure 4-d). There are little differences (mostly
422 insignificant) between under canopy and open fSCA at Sagehen on March 26, 2016, in the colder
423 T_{DJF} bands (T_{DJF} < -1.8°C), because fSCA is close to 100% (Figure 4-a). As snowmelt
424 progresses into April and May at Sagehen, fSCA declines and it becomes greater in the open
425 than under canopy in all but the coldest bands (T_{DJF} < -2°C), where fSCA remains close to 100%.

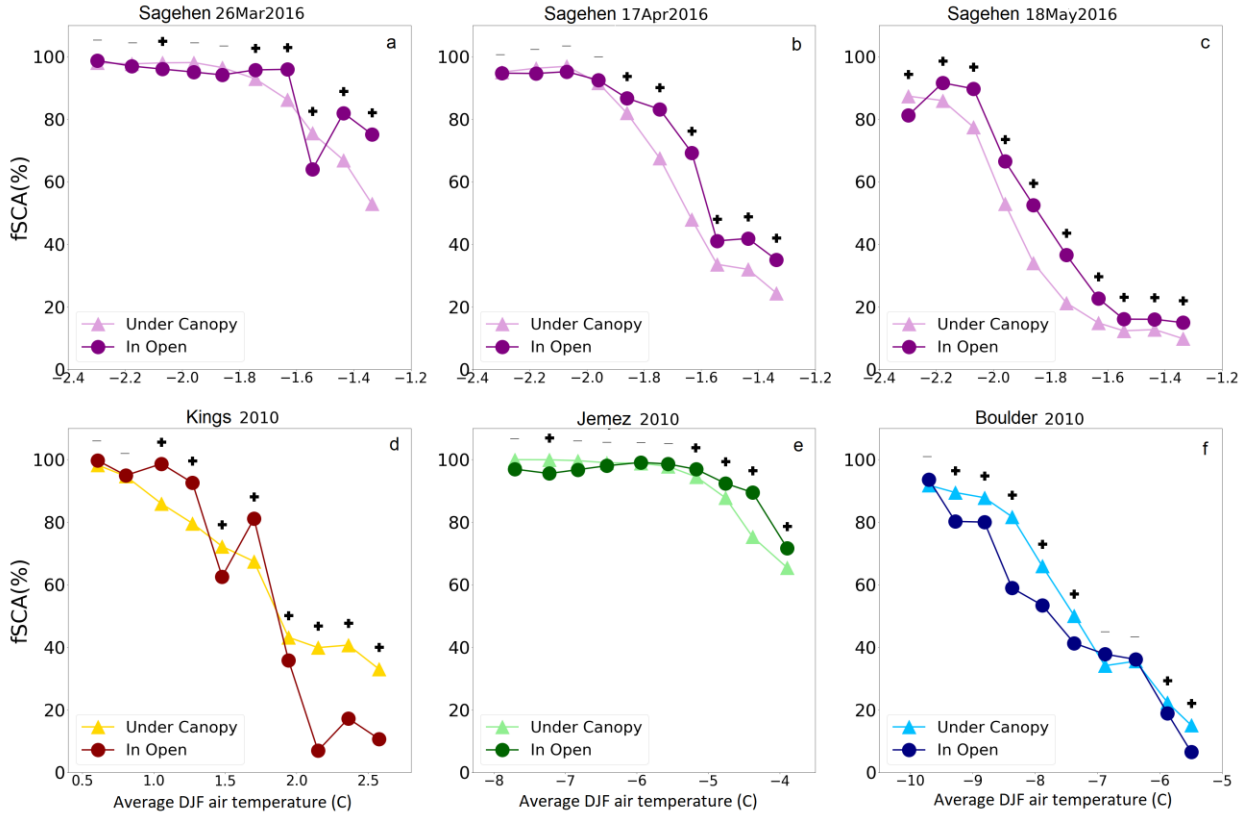

426

427 Figure 4: Under canopy and open fSCA in each T_{DJF} band for lidar flights over Sagehen on
428 March 26, April 17 and May 18, 2016 (a, b, c), Kings in March 2010 (d), Jemez in April 2010
429 (e), and Boulder in May 2010 (f). "+" signs in all panels represent statistically different under
430 canopy and open fSCA, based on Wilcoxon signed-rank test. Note that the x axes are different
431 for each site.

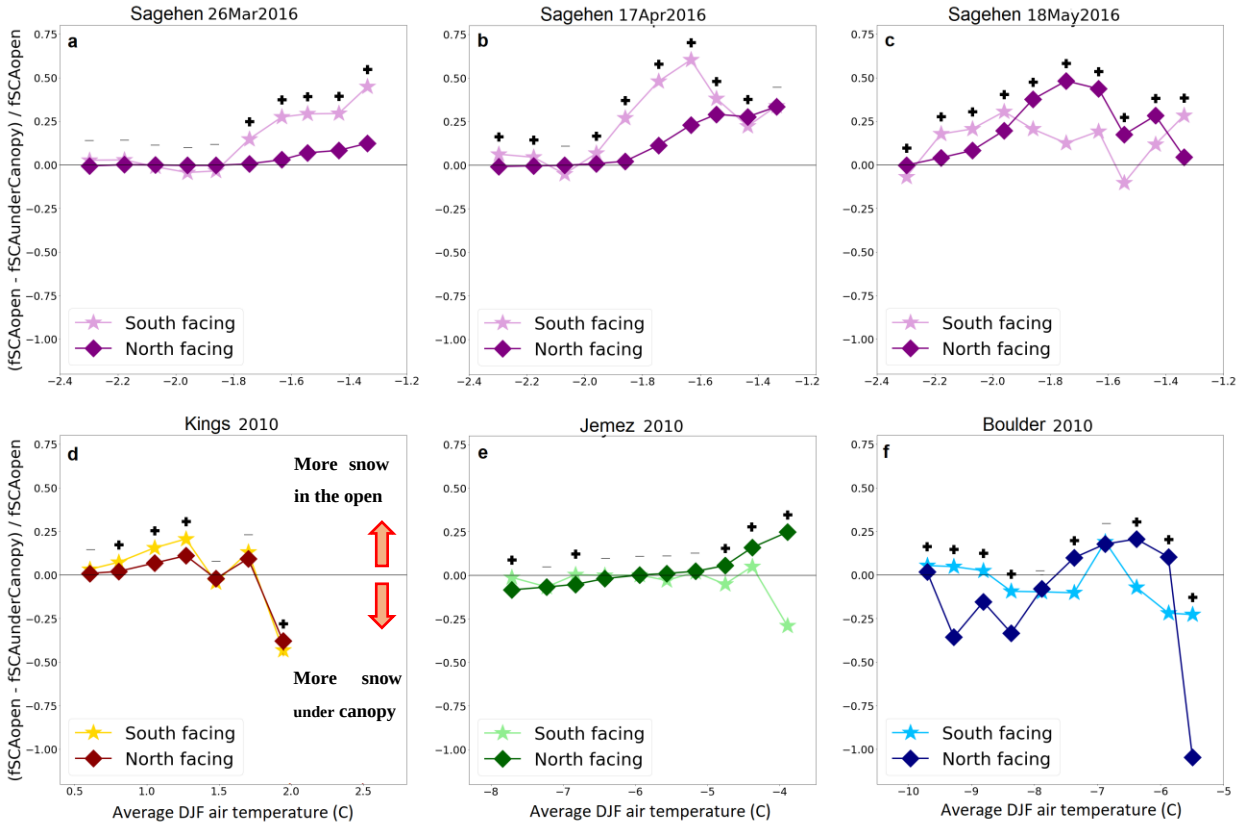

Figure 5: [$fSCA_{open}$ – $fSCA_{underCanopy}$]/ $fSCA_{open}$ for south-facing and north-facing slopes over different T_{DJF} bands for each Lidar flight over Sagehen in March 26, April 17 and May 18, 2016 (a, b, c); Kings in March 2010 (d); Jemez in April 2010 (e); and Boulder in May 2010 (f). "+" signs indicate statistically significant difference between [$fSCA_{open}$ – $fSCA_{underCanopy}$]/ $fSCA_{open}$ (y axis value) in south- and north-facing slopes.

Figure 5 depicts the ratio of the difference in open and under canopy fSCA to the open fSCA (i.e. [$fSCA_{open}$ – $fSCA_{underCanopy}$]/ $fSCA_{open}$) for south-facing (northness<-0.1) and north-facing (northness>0.1) slopes over different T_{DJF} bands for the different lidar flights and sites. Each site shows different interactions with elevation and slope/aspect; however, north-facing slopes have consistently higher fSCA than south-facing slopes (not showed in Figure 5). Generally, south-facing slopes show greater differences between open and under canopy fSCA than north facing slopes in most of the sites. At the coldest Boulder site and in the coldest T_{DJF} bands (T_{DJF} < -9°C) fSCA is higher in the open than under canopy in south-facing slopes (Figure 5-f). Conversely, north-facing slopes in colder bands (T_{DJF} < -8°C) at Boulder have higher under canopy fSCA

than open fSCA (except for the colder T_{DFJ} band). In warmer T_{DJF} bands at Boulder (T_{DJF} > -7.5°C), open fSCA is higher than under canopy on north-facing slopes (except for the warmest T_{DFJ} band), but opposite on south-facing slopes (Figure 5-f). Colder T_{DJF} bands (T_{DJF} < -5°C) at Jemez show virtually no differences between open and under canopy fSCA in either south-facing or north-facing slopes. Warmer T_{DJF} bands at Jemez act similar to warmer parts of Boulder, fSCA in the open is higher than under canopy on north-facing slopes and vice versa for south-facing slopes (Figure 5-e). In Kings, fSCA in the open is higher than under canopy in colder T_{DJF} bands, but reverses in warmer T_{DJF} bands (Figure 5-d) across north and south-facing slopes. At Sagehen, open fSCA is higher than under canopy fSCA on both north-facing and south-facing slopes for most warmer bands (T_{DJF} >-2 C) during March and April 2016 (Figure 5-a-b).

4.3 Lidar-derived relationships of snow retention differences and forest structure

We classify fSCA as either low vegetation density (lowVD, 0.01<vegetation density<0.4) or high vegetation density (highVD, vegetation density>0.6) for each site (Figure 6). In general, under canopy fSCA is higher under lowVD compared to highVD (Figure 6) on both north and south-facing slopes, except for south-facing slopes in Jemez. In the colder Boulder and Jemez sites, over colder T_{DJF} bands (T_{DJF} < -6.5°C for Boulder, and T_{DJF} < -4.5°C for Jemez), this pattern is more prevalent; while in warmer T_{DJF} bands, fSCA is higher under highVD for both south- and north-facing slopes (Figure 6-e and 6-f). At the warmest Kings site and the warmest T_{DJF} bands (T_{DJF} > 2°C) fSCA is highest under highVD in south-facing slopes and lowest under lowVD in north-facing slopes (Figure 6-d). At Sagehen over all T_{DJF} bands, there is a large difference between fSCA on south-facing and north-facing slopes under either lowVD or highVD (Figure 6-a, 6-b and 6-c). This difference between fSCA on south- and north-facing slopes at Sagehen increases in warmer months and warmer T_{DJF} bands. fSCA at Sagehen is highest in north-facing slopes under lowVD and lowest in south-facing slopes under highVD. The effects of canopy and slope/aspect converge in May as fSCA approaches zero in warmer T_{DJF} bands (T_{DJF} > -1.5°C) (Figure 6-c).

Here we explored the impact of two vegetation density classifications on fSCA which does not completely indicate the importance of vegetation density. Since vegetation density should be considered as a continuous variable, We develop a Random Forest model (RFM) to isolate the

effects of vegetation density, in addition to average incoming shortwave (SWR) and longwave (LWR), precipitation (P), and temperature (T) in fSCA differences between paired under canopy and open areas.

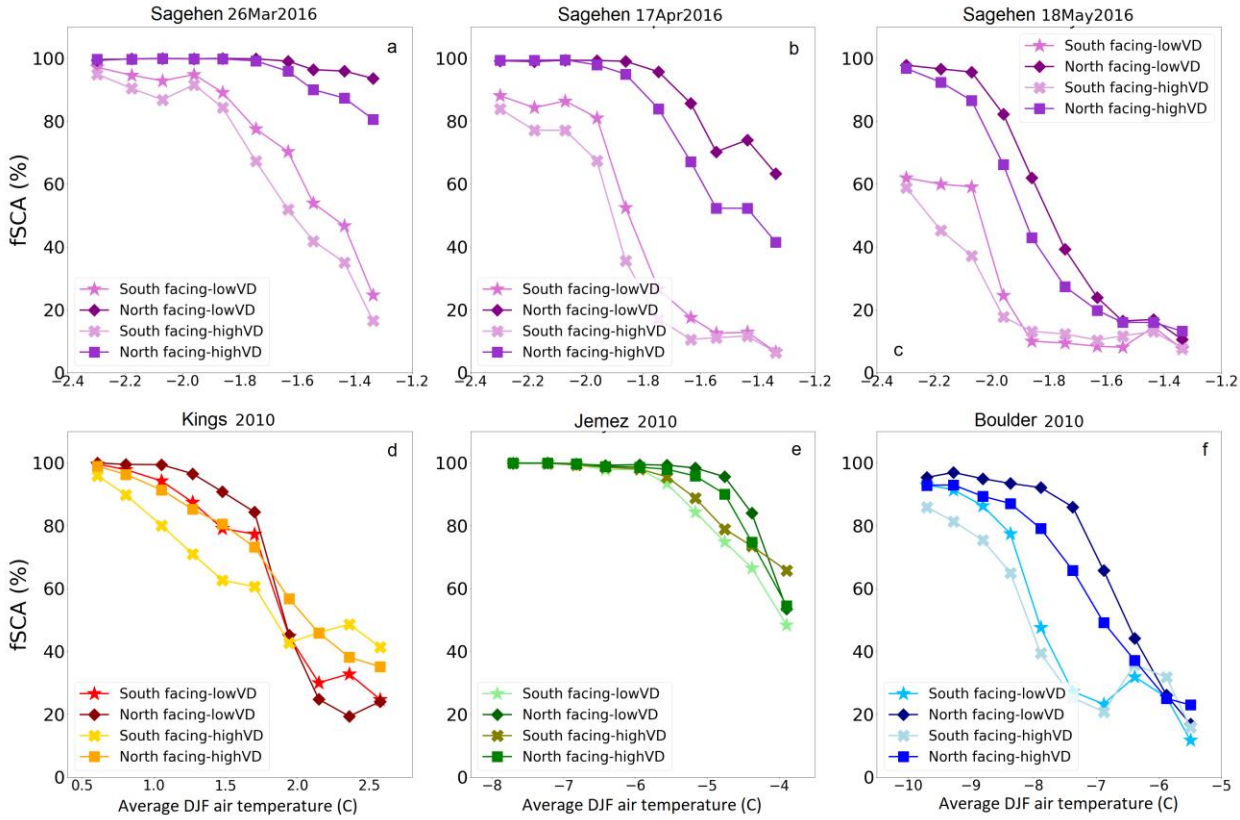

Figure 6: Under canopy fSCA for south-facing and north-facing slopes with low and high vegetation density (lowVD and highVD, respectively) across T_{DJF} bands for each lidar flight over Sagehen in March 26, April 17 and May 18, 2016 (a, b, c), Kings in March 2010 (d), Jemez in April 2010 (e), and Boulder in May 2010 (f).

4.4 Inferring controls on differences between under canopy and open fSCA with a Random Forest model

We develop a Random Forest model (RFM) to predict fSCAopen – fSCAunderCanopy from the same 100-m grid cell. The average RFM mean absolute errors (MAEs) for Sagehen in March 26, April 17 and May 18, 2016, Kings, Jemez, and Boulder are 0.07, 0.06, 0.05, 0.12, 0.10, and 0.11 (absolute fSCA units, i.e. fractions or %), respectively. The RFM indicates that vegetation

density is the most important variable for predicting fSCA differences in the colder sites (Figure 7). However, the role of vegetation density generally declines with declining fSCA across sites. In general, the influence of LWR and SWR on controlling fSCA differences in open and under canopy areas is same as the influence of vegetation density at warmer and lower fSCA bins at Kings and Sagehen (Figure 7a-d). The importance of precipitation and temperature is largest in the lowest fSCA bins, except for Sagehen (Figure 7).

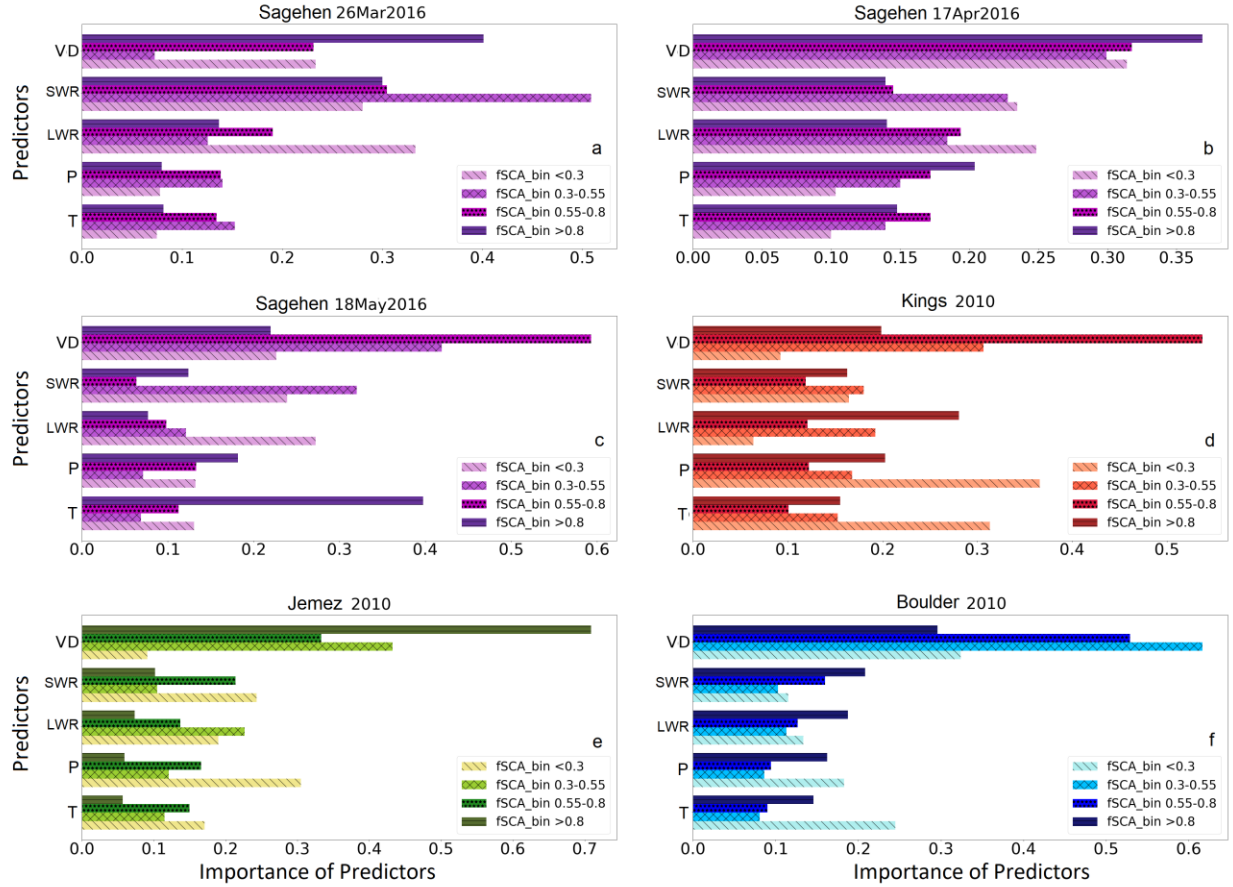

Figure 7: Importance of five predictors: vegetation density (VD), average incoming shortwave (SWR) and longwave (LWR) radiation, total precipitation (P) and average temperature (T), from December 1st to the day of lidar overflights for predicting [$fSCA_{open}$ - $fSCA_{underCanopy}$] in fSCA bins of fSCA<0.3, 0.3<=fSCA<0.55, 0.55<=fSCA<0.8 and 0.8<=fSCA for each lidar flight: Sagehen in March 26, April 17 and May 18, 2016 (a, b, c), Kings in March 2010 (d), Jemez in April 2010 (e), and Boulder in May 2010 (f).

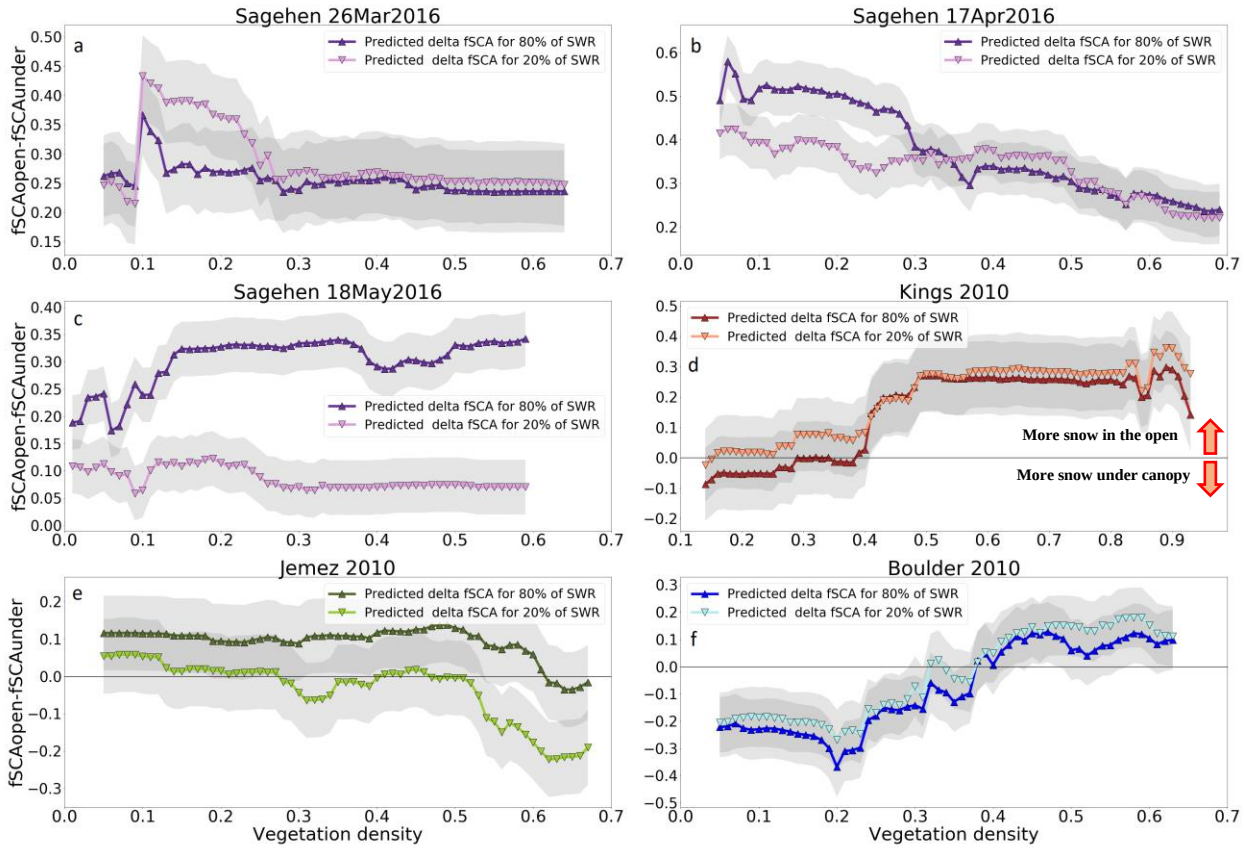

Figure 8: Prediction of [$fSCA_{open}$ – $fSCA_{underCanopy}$] across all sites using the RFM for 20th and 80th percentile of mean DJF incoming SWR across different vegetation densities, and the mean of incoming LWR, precipitation and temperature for each lidar flight over Sagehen in March 26, April 17 and May 18, 2016 (a, b, c), Kings in March 2010 (d), Jemez in April 2010 (e), and Boulder in May 2010 (f).

We use the RFM models to predict the difference between open and under canopy fSCA for the 0.3<fSCA<0.8 bin across vegetation density (Figure 8). The 20th and 80th percentile of SWR data and the mean of all other predictor variables is used to represent low and high insolation environments. We select 90 as a minimum number of 100-m grid cells; if the number of 100-m grid cells is less than 90, we do not show in Figure 8. Most of the sites do not have at least 90 grid cells with vegetation density>0.7 (except for Kings), hence the maximum number is 0.7 in x-axis in Figure 8, with the exception of Kings. fSCA in the open is higher than under canopy across all vegetation densities at the warm sites of Kings and Sagehen, with an exception of 80th percentile of SWR scenario in lower vegetation density (<0.4) at Kings. The RFM models show fundamental differences among colder sites, such as higher fSCA under canopy than open across

lower vegetation density areas at Boulder and the opposite effect of vegetation density at Jemez. Areas with higher vegetation density (vegetation density > 0.4) generally have higher open fSCA relative to under canopy fSCA at all sites except for Jemez. Similarly, as vegetation density approaches ~0.4, differences between open and under canopy fSCA stabilize at all sites except Jemez and April 17 in Sagehen to a lesser degree. It is worth noting the Jemez site had the largest relative uncertainties in fSCA prediction (Figure 8).

5 Discussion

Leveraging a new method of snow-on airborne lidar analysis into a multi-site analysis allows for new process insights into the causes of inter- and intra-site differences in open vs. under canopy snow retention. Our smallest lidar dataset has 2.6 million 1-m^2 grid cells (Kings), compared to the typical small sample size of around ~5-10 ground-based sensors per site (Figure 2). Lidar surveys have an obvious advantage for accurate determination of snow presence or absence spatially, though only provides a snapshot in time; whereas ground-based observations provide a continuous time-series over a much smaller domain. Large extent lidar datasets from multiple sites present opportunities to investigate snow processes over wide elevation and slope/aspect gradients at sites with various climates that are infeasible with ground-based measurements. The large number of points also provides statistical power (i.e. decreases noise/uncertainties), that otherwise could be overwhelming the signal with only a small ground-based dataset. As the availability of snow-on lidar datasets increases (Deems et al., 2013; Painter et al., 2016), the method pioneered by Kostadinov et al. (2019) can be improved and expanded in several ways. For example, the detection of snow surface versus low canopy branches is a fundamental challenge in very dense canopy unless the method or datasets are improved. Sites with multi-temporal snow-on lidar datasets (like Sagehen ASO flights, Painter et al., 2016) offer the potential to track fSCA (or snow disappearance) directly, which was only preliminarily explored here. Collection of additional lidar datasets could expand and improve our method, facilitating our understanding of snow retention that were not possible with other existing datasets.

In contrast to previous conceptual models, our findings suggest that local site characteristics, like vegetation density, can be a greater driver of differences in under canopy and open snow retention than climatic factors, like winter air temperature (Lundquist et al., 2013). For example,

548 at the coldest and windiest Boulder site we observe that increased vegetation density leads to a
549 shift from greater snow retention under canopy at lower vegetation density to greater snow
550 retention in open at high vegetation density. We show that open fSCA is higher than under
551 canopy fSCA at Jemez where T_{DJF} is between -5.5 to -4 ^{o}C (Figure 4). Ground-based sensors are
552 impractical for observing snow presence across gradients of vegetation density. Vegetation
553 density was shown to be the primary predictor of fSCA differences by the RFM (Figure 7),
554 suggesting that, in general, denser forests cause earlier snow disappearance under canopy
555 regardless of climate or slope and aspect (Figure 6 and 8). The lidar-based method shows
556 interesting patterns that have been challenging to detect with ground observations, like a shift
557 from greater snow retention under low vegetation density during mid-melt season to greater
558 snow retention under high vegetation density at the end of melt season at Kings and parts of
559 Jemez (Figure 6). These novel observations of fSCA in open and under canopy areas allow for
560 new insights into the competition between snow accumulation and ablation processes across
561 gradients in topography and vegetation density.

562 Our results suggest that the processes controlling open and under canopy snow retention are
563 strongly influenced by the interaction of vegetation structure and topography. Generally,
564 sheltering from wind and shortwave radiation (SWR) increases under canopy snow retention,
565 whereas longwave radiation (LWR) enhancement and snow interception decrease under canopy
566 snow retention (Lundquist et al., 2013). Tree canopy can emit more LWR than the surrounding
567 atmosphere, which efficiently ablates the snowpack at sites like Sagehen in forest patches where
568 vegetation density is >0.4 and air temperatures are relatively warm (Todt et al., 2018; Webster et
569 al., 2017). LWR is likely the dominant energy flux during the ablation at the warmer sites (Todt
570 et al., 2018). Denser canopies also intercept more snowfall, leading to lower SWE and less
571 energy required to melt the snowpack. Interception of warm snowfall is higher than cold
572 snowfall or rain (Roth and Nolin, 2017), which is consistent with greater interception (and lower
573 under canopy fSCA) at warmer sites, implied by Figure 8. Forest canopy also reduces wind
574 speed and turbulent energy fluxes at the snowpack surface (Kremsa et al., 2015), decreases
575 blowing snow sublimation and redistribution, and thus, increases under canopy fSCA
576 (Dickerson-Lange et al., 2017, Tennant et al., 2017). We infer wind sheltering from canopy as an
577 important driving mechanism at our windiest site Boulder, where fSCA under canopy is higher

than in the open (Erickson et al., 2005). Shading effects from SWR is the highest on south-facing slopes in early summer when solar zenith angle is lower (Strasser et al., 2011). Surprisingly, increased SWR on south-facing slopes causes greater ablation under canopy at colder sites because of inferred interception and LWR enhancement of warmer, dense vegetation (vegetation density>0.4) (Todt et al., 2018; Webster et al., 2017) (Figure 8). Vegetation density and topography mediate the feedbacks between SWR and LWR, which is outside of previous temperature-based frameworks for predicting snow retention (Lundquist et al. 2013). Interestingly, both warm and cold sites show relatively little sensitivity to energy and mass budgets when vegetation density is greater than 0.6 (i.e. leveling off in Figure 8), with the exception of Jemez. We interpret that the relationship of the canopy interception efficiency and canopy emissivity saturate at high vegetation densities; although there are relatively few 100-m areas with high vegetation density (Figure 8). It is worth noting that open forest areas can be differentially shaded by the adjacent trees, depending on forest height and density (Musselman et al., 2015). Future studies may consider a more exact definition of an open site, or a better definition that considers the adjacent forest canopy. Overall, our inferences are consistent with snow-forest processes that control differences between open and under canopy fSCA, and provide a better understanding of snow retention across gradients of climate, topography and vegetation structure.

We develop a new conceptual framework that takes advantage of our process insights to better explain how topography and vegetation structure interact to control open and under canopy snow retention across sites with different climates. Despite relationships between air temperature and snowpack energy fluxes (Ohmura, 2001), differences between open and under canopy fSCA are not well predicted by thresholds in TDJF. More snow retention in open compared to nearby under canopy areas is found when TDJF varies between -4.5 to 1.5 oC, likely because LWR from warm canopy is more important (Table 3). Denser tree cover intercepts more snowfall and has greater thermal mass, causing greater snow retention in open compared to under canopy locations, specifically at warm sites (Table 3). Areas warmer than 2 °C experience higher under canopy snowpack in the melt season (i.e. Kings; Figure 4, 5; table 3), suggesting that later persisting snowpack may experience a transition from LWR- to SWR-limited retention as the solar zenith angle decreases. Interception, wind effects, and shading from SWR are the

608 dominant processes at the colder sites, leading to more variable snow retention dynamic
609 compared to the warmer sites. One of our key findings is that slope and aspect can accentuate or
610 mediate the effects of local climate on the snowpack energy budget. Snow retention is higher
611 under canopy on north-facing slopes in colder climates, where wind sheltering and SWR shading
612 are the dominant drivers. However, open area snow retention is higher than under canopy areas
613 in lower elevations in colder areas, indicating that LWR and efficient snow interception makes
614 these cold, low elevation areas behave more like 'warm' sites in the climate based Lundquist et
615 al. (2013) framework (Table 3). South-facing slopes accentuate the local energy budget and lead
616 to more consistent snow retention properties than north-facing slopes. For example, south-facing
617 slopes that receive substantial SWR have greater snow retention in open versus under canopy
618 areas than north facing slopes at Kings and Sagehen (Table 3). Only in the coldest and windiest
619 Boulder site we observe greater snow retention under lower vegetation density than under high
620 VD canopy, because of SWR and wind sheltering (Table 3).

621 Our new conceptual model, explaining the interacting energy-mass controls on differential snow
622 retention in open and under canopy locations, could inform forest management actions.
623 Increasing snow retention on the landscape delays the input of water, results in long recession in
624 soil moisture (Harpold and Molotch, 2015), and limits the water stress period for ecosystems
625 (Harpold, 2016). Later snowmelt similarly delays the dry down of surface fuels and thus, reduces
626 extreme wildfire activity (Westerling et al., 2006). Forest management actions (e.g. tree removal
627 and controlled fire) with the goal of retaining snow on the landscape have a long history
628 (Alexander et al., 1985; Anderson, 1983; Golding and Swanson, 1986; Varhola et al., 2010).
629 However, our insights using a lidar-derived dataset allow more spatially explicit management
630 strategies that account for natural variability of complex topography and forest structure. For
631 example, thinning or gap-cutting, which decreases LWR and canopy snow interception, could
632 help retain snowpack at the warm and dense canopy sites of Sagehen. Similarly, lower elevations
633 of colder areas may experience limited snow retention benefits of tree removal (e.g. Boulder).
634 However, colder south-facing slopes with low canopy density (especially at higher, windier
635 elevations) might experience reductions in snow retention following tree removal from fire or
636 thinning. There remains potential to expand the machine learning (i.e. RFM) approaches to better
637 infer process insights that take advantage of multi-temporal and multi-site datasets. Moreover, an

approach that moves beyond binary classifications (e.g. vegetation density, open versus under canopy, etc.) might provide better understanding of controlling processes. We believe our conceptual framework offers an important advancement in our understanding of snow retention in montane forests that should be refined with new process-based knowledge. An important future step will be to apply snowpack energy balance models to better identify physical mechanisms controlling differential snow retention.

Table 3: Conceptual model illustrating how the interactions between vegetation structure, topography and climate shape the energy and mass budgets resulting in differences in snow cover between open and under canopy.

Canopy density	**Mass & energy drivers in warmer areas**		**Mass & energy drivers in colder areas**	
Lower vegetation density (LowVD) 	**South facing slopes (SF)** 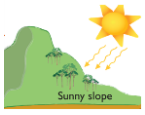	❖ **More snow in open (more than NF slopes)** ✓ **LWR dominates** ✓ **Lower snow Interception efficiency compared to NF slopes and HighVD** ➢ **RFL*:** • Sagehen26Mar, ER*: 1940-2560 MASL • Sagehen17Apr, ER: 2130-2560 MASL • Sagehen18May, ER: 2370-2560 MASL • Kings ER: 1650-2050 MASL	**South facing slopes (SF)** 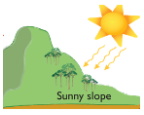	❖ **More snow under canopy** ✓ **Shading from SWR** ➢ **RFL** • Boulder, EL: 2800-3220 MASL • Boulder, ER: lower than 2775 MASL • Jemez, ER: lower than 2800 MASL
	North facing slopes (NF) 	❖ **More snow in open** ✓ **LWR effect** ✓ **Less SWR exposure** ✓ **Higher interception efficiency compared to SF slopes** ➢ **RFL:** • Sagehen26Mar, ER: 1940-2560 MASL • Sagehen17Apr, ER: 2130-2560 MASL • Sagehen18May, ER: 2130-2560 MASL • Kings ER: 1750-2050 MASL	**North facing slopes (NF)** 	❖ **In higher elevation more snow under canopy** ✓ **Shading from SWR** ✓ **Less SWR exposure** ✓ **Wind sheltering** ➢ **RFL:** • Jemez, ER: 2650-3400 MASL • Boulder, ER: 2800-3220 MASL ❖ **In lower elevation, more snow in open** ✓ **Less SWR exposure** ✓ **LWR effect** ✓ **Fairly efficient interception** ➢ **RFL:** • Jemez, ER: lower than 2600 MASL

Table 3-continued: Conceptual model illustrating how vegetation structure and topographic features interact with climate to shape energy budget resulting in higher snow cover in the open or under canopy.

Canopy density	Mass & energy drivers in warmer areas		Mass & energy drivers in colder areas	
Higher vegetation density (HighVD) 	**South facing slopes (SF)** 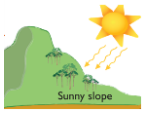	❖ **More snow in open (more than NF slopes; less than LowVD)** ✓ **LWR dominates** ✓ **Efficient Interception** ➢ **RFL:** • Sagehen26Mar, ER: 1940-2560 MASL • Sagehen17Apr, ER: 2130-2560 MASL • Sagehen18May, ER: 2370-2560 MASL • Kings ER: 1650-2050 MASL	**South facing slopes (SF)** 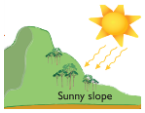	❖ **More under the canopy** ✓ **Shading from SWR dominates** ✓ **Fairly efficient interception** ✓ **Higher wind sheltering** ➢ **RFL:** • Jemez, ER: lower than 2800 MASL • Boulder, ER: lower than 2775 MASL
	North facing slopes (NF) 	❖ **More snow in open (less than LowVD)** ✓ **LWR effect** ✓ **Less SWR exposure** ✓ **Most efficient Interception compared to SF slopes** ➢ **RFL:** • Sagehen26Mar, ER: 1940-2560 MASL • Sagehen17Apr, ER: 2130-2560 MASL • Sagehen18May, ER: 2130-2560 MASL • Kings ER: 1750-2050 MASL	**North facing slopes (NF)** 	❖ **In higher elevation more snow under canopy** ✓ **Shading from SWR** ✓ **Highest Wind sheltering** ✓ **Most efficient interception** ➢ **RFL:** • Jemez, ER: 2650-3400 MASL • Boulder, ER: 2800-3220 MASL ❖ **In lower elevation, more snow in open** ✓ **Less SWR exposure** ✓ **LWR effect** ✓ **Efficient interception** ➢ **RFL:** • Jemez, ER: lower than 2600 MASL • Boulder, ER: lower than 2775 MASL

*RFL: reference locations; ER: elevation range.

Orange color shows more snow in the open; **green color** shows more snow under canopy; and **purple color** shows mass and energy budget processes that drive snow dynamics.

654

655

656 6 Conclusions

657 Altering forest canopy structure is one of the few ways to control the timing of snow
658 disappearance and its ecohydrological consequences. Our new conceptual framework shows that
659 areas where longwave radiation (LWR) and snow interception dominate, are characteristic of
660 'warm' climate and have less snow under canopy versus in the open. Conversely, colder areas
661 where shortwave radiation (SWR) and turbulent energy fluxes are the main drivers, can have
662 greater under canopy snowpack. This indicates that forest disturbances that reduce canopy cover
663 will have different effects under different local climate, but in ways that are strongly mediated by
664 topography. Colder and denser forests are likely to experience tradeoffs between interception,
665 reducing snow retention, and SWR and wind sheltering (Varhola et al., 2010). This is consistent
666 with the lack of snowpack response to tree removal in the Rocky Mountains in previous studies
667 of insect-caused tree mortality (Biederman et al., 2014) and fire caused canopy loss (Harpold et
668 al., 2014). This makes the effects of vegetation disturbance on snowpack highly dependent on
669 the remaining vegetation and its co-variation with slope-aspect and elevation. In warmer areas
670 more efficient LWR and snow interception work together to reduce snowpack cold content and
671 increase ablation. Therefore, warmer areas with dense vegetation typically have potential for
672 canopy removal to increase snow retention, especially on south-facing slopes. These process
673 inferences have the potential to be strengthened by expanding to additional sites and times during
674 the ablation season, as well as pre- and post-disturbance investigations. Given the few tools
675 available to monitor under canopy snow disappearance over large spatial extents, lidar-based
676 inferences should prove critical to improve our predictive models of snow-forest interactions in a
677 changing world.

678 All snow-on and snow-off lidar datasets for Jemez, Boulder and Kings and snow-off lidar dataset
679 for Sagehen are freely available from https://portal.opentopography.org/datasets public data
680 servers.

Acknowledgments

This project was supported by the California Wildlife Conservation Board Stream Flow Enhancement Program. The lidar surveys were funded by the National Science Foundation (NSF) for a common project between the National Center for Airborne Laser Mapping (NCALM) and the Critical Zone Observatory (CZO) program (http://opentopo.sdsc.edu/datasets). We thank Dr. Tom Painter and the Airborne Snow Observatory for the lidar data from Sagehen. We thank Jeff Brown and Dan Sayler at Sagehen Creek Field Station and Dr. Jessica Lundquist and Susan Dickerson-Lange for the helpful conversations over the past several years. We thank Dr. Scott Tyler and Rowan Gaffney for help deploying and maintaining the DTS equipment. We appreciate the field observations provided by the CZO program and the work of Drs. Noah Molotch, Roger Bales, and Paul Brooks.

References

Alexander, R. R., C. A. Troendle, M. R. Kaufmann, W. D. Shepperd, G. L. Crouch, and R. K. Watkins, (1985). The Fraser Experimental Forest, Colorado: Research program and published research 1937–1985. USDA Forest Service General Tech. Rep. RM-118, Rocky Mountain Forest and Range Experiment Station, Fort Collins, CO, 46.

Amatulli, G., Domisch, S., Tuanmu, M. Tuanmu M., Parmentier B., Ranipeta A., Malczyk J. and Jetz W. (2018). A suite of global, cross-scale topographic variables for environmental and biodiversity modeling. Sci Data 5, 180040.

Anderson, E. (1976). A point energy and mass balance model of snow cover. NOAA Technical Report NWS 19, U.S. National Weather Service, Dept. of Commerce, Washington, DC.

Bach, A. F., G. van der Schrier, L. A. Melsen, A. Tank, and A. J. Teuling (2018). Widespread and Accelerated Decrease of Observed Mean and Extreme Snow Depth Over Europe, Geophysical Research Letters, 45(22), 12312-12319.

Bales, R. C., J. W. Hopmans, A. T. O'Geen, M. Meadows, P. C. Hartsough, P. Kirchner, C. T. Hunsaker, and D. Beaudette (2011). Soil Moisture Response to Snowmelt and Rainfall in

a Sierra Nevada Mixed-Conifer Forest, Vadose Zone Journal, 10(3), 786-799.

Barnett, T. P., J. C. Adam, and D. P. Lettenmaier (2005). Potential impacts of a warming climate on water availability in snow-dominated regions, Nature, 438(7066), 303-309.

Biederman J.A., P. D. Brooks, A. A. Harpold, D. J. Gochis, E. Gutmann, D. E. Reed, E. Pendall, B. E. Ewers (2014). Multiscale observations of snow accumulation and peak snowpack following widespread, insect-induced lodgepole pine mortality. Ecohydrology 7(1):150–162.

Blankinship, J. C., E. P. McCorkle, M. W. Meadows, and S. C. Hart (2018). Quantifying the legacy of snowmelt timing on soil greenhouse gas emissions in a seasonally dry montane forest, Global Change Biology, 24(12), 5933-5947.

Broxton, P. D., A. A. Harpold, J. A. Biederman, P. A. Troch, N. P. Molotch, and P. D. Brooks (2015). Quantifying the effects of vegetation structure on snow accumulation and ablation in mixed-conifer forests, Ecohydrology, 8(6), 1073-1094.

Cawley C. G. and N. L. C. Talbot (2010). On Over-fitting in Model Selection and Subsequent Selection Bias in Performance Evaluation, Journal of Machine Learning Research, 11 (2079-2107).

Conner, L. G., R. A. Gill, and J. Belnap (2015). Soil moisture response to experimentally altered snowmelt timing is mediated by soil, vegetation, and regional climate patterns, Ecohydrology, 9(6), 1006-1016.

Coons, L.P., Nolin, A.W., Gleason, K.E., Mar, E.J., Rittger, K., Roth, T.R., Painter, T.H., (2014). Seeing the snow through the trees: toward a validated canopy adjustment for satellite snow-covered area. In: Remote Sensing of the Terrestrial Water Cycle, pp. 199–213.

Cooper, M. G., A. W. Nolin, and M. Safeeq (2016). Testing the recent snow drought as an analog for climate warming sensitivity of Cascades snowpacks, Environmental Research Letters, 11(8).

Deems, J. S., T. H. Painter, and D. C. Finnegan (2013). Lidar measurement of snow depth: a

review, Journal of Glaciology, 59(215), 467-479.

Dibike, Y., H. I. Eum, and T. Prowse (2018). Modelling the Athabasca watershed snow response to a changing climate, Journal of Hydrology-Regional Studies, 15, 134-148.

Dickerson-Lange, S. E., J. A. Lutz, R. Gersonde, K. A. Martin, J. E. Forsyth, and J. D. Lundquist (2015a). Observations of distributed snow depth and snow duration within diverse forest structures in a maritime mountain watershed, Water Resources Research, 51(11), 9353-9366.

Dickerson-Lange, S. E., J. A. Lutz, K. A. Martin, M. S. Raleigh, R. Gersonde, and J. D. Lundquist (2015b). Evaluating observational methods to quantify snow duration under diverse forest canopies, Water Resources Research, 51(2), 1203-1224.

Dickerson-Lange, S. E., R. F. Gersonde, J. A. Hubbart, T. E. Link, A. W. Nolin, G. H. Perry, T. R. Roth, N. E. Wayand, and J. D. Lundquist (2017). Snow disappearance timing is dominated by forest effects on snow accumulation in warm winter climates of the Pacific Northwest, United States, Hydrological Processes, 31(10), 1846-1862.

Ellis, C. R., J. W. Pomeroy, R. L. H. Essery, and T. E. Link (2011). Effects of needleleaf forest cover on radiation and snowmelt dynamics in the Canadian Rocky Mountains, Can. J. Forest Res., 41(3), 608–620, doi:10.1139/X10-227.

Erickson, T. A., Williams, M. W. and Winstral, A. (2005). Persistence of topographic controls on the spatial distribution of 596 snow in rugged mountain terrain, Colorado, United States, Water Resour. Res., 41(4), W04014.

Freudiger, D., I. Kohn, J. Seibert, K. Stahl, and M. Weiler (2017). Snow redistribution for the hydrological modeling of alpine catchments, Wiley Interdisciplinary Reviews-Water, 4(5).

Fujihara, Y., K. Takase, S. Chono, E. Ichion, A. Ogura, and K. Tanaka (2017). Influence of topography and forest characteristics on snow distributions in a forested catchment, Journal of Hydrology, 546, 289-298.

759 Golding, D. and Swanson, R. (1986). Snow Distribution Patterns in Clearings and Adjacent
760 Forest. Water Resources Research - WATER RESOUR RES. 22. 1931-1940.
761 10.1029/WR022i013p01931.

762 Harder, P., J. W. Pomeroy, and W. D. Helgason (2019). A simple model for local-scale sensible
763 and latent heat advection contributions to snowmelt, Hydrology and Earth System
764 Sciences, 23(1), 1-17.

765 Harpold, A. A. (2016). Diverging sensitivity of soil water stress to changing snowmelt timing in
766 the Western US, Advances in Water Resources, 92, 116-129.

767 Harpold, A. A., and N. P. Molotch (2015). Sensitivity of soil water availability to changing
768 snowmelt timing in the western US, Geophysical Research Letters, 42(19), 8011-8020.

769 Harpold, A. A., N. P. Molotch, K. N. Musselman, R. C. Bales, P. B. Kirchner, M. Litvak, and P.
770 D. Brooks (2015a). Soil moisture response to snowmelt timing in mixed-conifer
771 subalpine forests, Hydrological Processes, 29(12), 2782-2798.

772 Harpold, A. A., J. A. Biederman, K. Condon, M. Merino, Y. Korgaonkar, T. Nan, L. L. Sloat, M.
773 Ross, and P. D. Brooks. (2014). Changes in snow accumulation and ablation following
774 the Las Conchas forest fire, New Mexico, USA. Ecohydrology 7:440–452.

775 Harpold, A. A., J. A. Marshall, S. W. Lyon, T. B. Barnhart, B. A. Fisher, M. Donovan, K. M.
776 Brubaker, C. J. Crosby, N. F. Glenn, C. L. Glennie, P. B. Kirchner, N. Lam, K. D.
777 Mankoff, J. L. McCreight, N. P. Molotch, K. N. Musselman, J. Pelletier, T. Russo, H.
778 Sangireddy, Y. Sjöberg, T. Swetnam, and N. West (2015b). Laser vision: lidar as a
779 transformative tool to advance critical zone science, Hydrology and Earth System
780 Sciences, 19(6), 2881-2943.

781 Huntington, J. L., and R. G. Niswonger (2012). Role of surface-water and groundwater
782 interactions on projected summertime streamflow in snow dominated regions: An
783 integrated modeling approach, Water Resour. Res., 48, W11524, doi:10.1029/
784 2012WR012319.

785 Jonas, T., Essery, R., (2011). Snow cover and snowmelt in forest regions. In: Singh, V.P.,
786 Haritashya, U.K. (Eds.), Encyclopedia of Snow, Ice and Glaciers. Series: Encyclopedia of
787 Earth Sciences Series. Springer, Dordrecht, Heidelberg, pp. 1033–1036.

788 Knowles, J. F., S. P. Burns, P. D. Blanken, and R. K. Monson (2015). Fluxes of energy, water,
789 and carbon dioxide from mountain ecosystems at Niwot Ridge, Colorado, Plant Ecology
790 & Diversity, 8(5-6), 663-676.

791 Kormos, P. R., D. Marks, F. B. Pierson, C. J. Williams, S. P. Hardegree, S. Havens, A. Hedrick,
792 J. D. Bates, and T. J. Svejcar (2017). Ecosystem Water Availability in Juniper versus
793 Sagebrush Snow-Dominated Rangelands, Rangeland Ecology & Management, 70, 116-
794 128.

795 Kostadinov, T. S., R. Schumer, M. Hausner, K. J. Bormann, R. Gaffney, K. McGwire, T. H.
796 Painter, S. Tyler, and A. A. Harpold (2019). Watershed-scale mapping of fractional snow
797 cover under conifer forest canopy using lidar, Remote Sensing of Environment, 222, 34-
798 49.

799 Kremsa, J., J. Krecek, and E. Kubin (2015). Comparing the impacts of mature spruce forests and
800 grasslands on snow melt, water resource recharge, and run-off in the northein boreal
801 environment, International Soil and Water Conservation Research, 3(1), 50-56.

802 Kumar L., A. K. Skidmore, and E. Knowles (2010). Modelling topographic variation in solar
803 radiation in a GIS environment. International Journal of Geographical Information
804 Science, 11 (5), 475-497.

805 Li, D. Y., M. L. Wrzesien, M. Durand, J. Adam, and D. P. Lettenmaier (2017). How much runoff
806 originates as snow in the western United States, and how will that change in the future?,
807 Geophysical Research Letters, 44(12), 6163-6172.

808 Lopez-Moreno, J. I., S. Gascoin, J. Herrero, E. A. Sproles, M. Pons, E. Alonso-González, L.
809 Hanich, A. Boudhar, K. N. Musselman, N. P. Molotch (2017). Different sensitivities of
810 snowpacks to warming in Mediterranean climate mountain areas, Environmental
811 Research Letters, 12(7).

812 Lundquist, J. D., S. E. Dickerson-Lange, J. A. Lutz, and N. C. Cristea (2013). Lower forest
813 density enhances snow retention in regions with warmer winters: A global framework
814 developed from plot-scale observations and modeling, Water Resources Research,
815 49(10), 6356-6370.

816 Malle, J., N. Rutter, G. Mazzotti, and T. Jonas (2019). Shading by Trees and Fractional Snow
817 Cover Control the Subcanopy Radiation Budget, Journal of Geophysical Research-
818 Atmospheres, 124(6), 3195-3207.

819 Maxwell, J. D., A. Call, and S. B. St Clair (2019). Wildfire and topography impacts on snow
820 accumulation and retention in montane forests, Forest Ecology and Management, 432,
821 256-263.

822 Moeser, D., G. Mazzotti, N. Helbig, and T. Jonas (2016). Representing spatial variability of
823 forest snow: Implementation of a new interception model, Water Resources Research,
824 52(2), 1208-1226.

825 Molotch, N. P., and L. Meromy (2014). Physiographic and climatic controls on snow cover
826 persistence in the Sierra Nevada Mountains, Hydrological Processes, 28(16), 4573-4586.

827 Molotch, N. P., and S.A., Margulis, (2008). Estimating the distribution of snow water equivalent
828 using remotely sensed snow cover data and a spatially distributed snowmelt model: a
829 multi-resolution, multi-sensor comparison. Adv. Water Resour. 31 (11), 1503–1514.

830 Musselman, K. N., and J. W. Pomeroy (2017). Estimation of Needleleaf Canopy and Trunk
831 Temperatures and Longwave Contribution to Melting Snow, Journal of
832 Hydrometeorology, 18(2), 555-572.

833 Musselman, K. N., J. W. Pomeroy, and T. E. Link (2015). Variability in shortwave irradiance
834 caused by forest gaps: Measurements, modelling, and implications for snow energetics,
835 Agricultural and Forest Meteorology, 207, 69-82.

836 O'Geen, A., M. Safeeq, J. Wagenbrenner, E. Stacy, P. Hartsough, S. Devine, Z. Tian, R. Ferrell,
837 J.W. Hopmans, and R. Bales (2018). Southern Sierra Critical Zone Observatory and

838 Kings River Experimental Watersheds: A Synthesis of Measurements, New Insights, and
839 Future Directions, Vadose Zone Journal, 17(1).

840 Ohmura, A. (2001). Physical basis for the temperature-based melt-index method, Journal of
841 Applied Meteorology 40, 753–761.

842 O'Leary, D. S., J. L. Kellermann, and C. Wayne (2018). Snowmelt timing, phenology, and
843 growing season length in conifer forests of Crater Lake National Park, USA, International
844 Journal of Biometeorology, 62(2), 273-285.

845 Painter, T. H., D. F. Berisford, J. W. Boardman, K. J. Bormann, J. S. Deem, F. Gehrke, A.
846 Hedrick, M. Joyce. R. Laidlaw, D. Marks, C. Mattmann, B. McGurk, P. Ramirez, M.
847 Richardson, S. M. Skiles, F. C. Seidel, A. Winstral (2016). The airborne snow
848 Observatory: Fusion of scanning lidar, imaging spectrometer, and physically-based
849 modeling for mapping snow water equivalent and snow albedo. Remote Sens. Environ.,
850 184, 139–152, doi:10.1016/j.rse.2016.06.018.

851 Pavlovskii, I., Hayashi, M., & Itenfisu, D. (2019). Midwinter melts in the Canadian prairies:
852 Energy balance and hydrological effects. Hydrology and Earth System
853 Sciences, 23, 1867–1883.

854 Pederseng, S. H., G. E. Liston, M. P. Tamstorf, J. Abermann, M. Lund, and N. M. Schmidt
855 (2018). Quantifying snow controls on vegetation greenness, Ecosphere, 9(6).

856 Peichl, M., J. Sagerfors, A. Lindroth, I. Buffam, A. Grelle, L. Klemedtsson, H. Laudon, and M.
857 B. Nilsson (2013). Energy exchange and water budget partitioning in a boreal
858 minerogenic mire, Journal of Geophysical Research-Biogeosciences, 118(1), 1-13.

859 Perrot, D., N. P. Molotch, K. N. Musselman, and E. T. Pugh (2014). Modelling the effects of the
860 mountain pine beetle on snowmelt in a subalpine forest, Ecohydrology, 7(2), 226-241.

861 Pomeroy, J. W., D. Marks, T. Link, C. Ellis, J. Hardy, A. Rowlands, and R. Granger (2009). The
862 impact of coniferous forest temperature on incoming longwave radiation to melting snow,
863 Hydrol. Processes, 23:(17), 2513–2525.

Raleigh, M. S., K. Rittger, C. E. Moore, B. Henn, J. A. Lutz, and J. D. Lundquist (2013). Ground-based testing of MODIS fractional snow cover in subalpine meadows and forests of the Sierra Nevada, Remote Sensing of Environment, 128, 44-57.

Revuelto, J., J. I. Lopez-Moreno, C. Azorin-Molina, and S. M. Vicente-Serrano (2015). Canopy influence on snow depth distribution in a pine stand determined from terrestrial laser data, Water Resources Research, 51(5), 3476-3489.

Roth, T. R., and A. W. Nolin (2017). Forest impacts on snow accumulation and ablation across an elevation gradient in a temperate montane environment, Hydrology and Earth System Sciences, 21(11), 5427-5442.

Seyednasrollah, B., M. Kumar, and T. E. Link (2013). On the role of vegetation density on net snow cover radiation at the forest floor, Journal of Geophysical Research-Atmospheres, 118(15), 8359-8374.

Slater, A. G., Schlosser, C. A., Desborough, C. E., Pitman, A. J., Henderson-Sellers, A., Robock, A., Vinnikov, K. Y., Mitchell, K., Boone, A., Braden, H., Chen, F., Cox, P. M., de Rosnay, P., Dickinson, R. E., Dai, Y.-J., Duan, Q., Entin, J., Etchevers, P., Gedney, N., Gusev, Y. M., Habets, F., Kim, J., Koren, V., Kowalczyk, E. A., Nasonova, O. N., Noilhan, J., Schaake, S., Shmakin, A. B., Smirnova, T. G., Verseghy, D., Wetzel, P., Xue, Y., Yang, Z.-L. and Zeng, Q. (2001). The representation of snow in land surface schemes: results from PILPS 2(d), Journal of Hydrometerology 2, 7–25.

Strasser, U., M. Warscher, and G. E. Liston (2011). Modeling Snow-Canopy Processes on an Idealized Mountain, Journal of Hydrometeorology, 12(4), 663-677.

Stueve, K.M., Perry, C.H., Nelson, M.D., Healey, S.P., Hill, A.D., Moisen, G.G.,Cohen, W.B., Gormanson, D.D., and Huang, C. 2011. Ecological importance of Intermediate windstorms rivals large, infrequent disturbances in the north-ern Great Lakes. Ecosphere, 2: art2.

Stevens J.T., Collins B.M., Miller J.D., North M.P., Stephens S.L. (2017). Changing spatial patterns of stand-replacing fire in California conifer forests, Forest Ecology and

Management 406: 28–36.

Stewart, I.T., Cayan, D.R. & Dettinger, M.D. (2004). Changes in Snowmelt Runoff Timing in Western North America under a `Business as Usual' Climate Change Scenario, Climatic Change 62: 217.

Storck P., Lettenmaier D. P., and Bolton S. M. (2002). Measurement of snow interception and canopy effects on snow accumulation and melt in a mountainous maritime climate, Oregon, United States. Water Resources Research, 38: 11.

Tennant, C. J., A. A. Harpold, K. A. Lohse, S. E. Godsey, B. T. Crosby, L. G. Larsen, P. D. Brooks, R. W. Van Kirk, and N. F. Glenn (2017). Regional sensitivities of seasonal snowpack to elevation, aspect, and vegetation cover in western North America, Water Resources Research, 53(8), 6908-6926.

Todt, M., N. Rutter, C. G. Fletcher, L. M. Wake, P. A. Bartlett, T. Jonas, H. Kropp, M. M. Loranty, and C. Webster (2018). Simulation of Longwave Enhancement in Boreal and Montane Forests, Journal of Geophysical Research-Atmospheres, 123(24), 13731-13747.

Tyler, S. W., Selker, J. S., Hausner, M. B., Hatch, C. E., Torgersen, T., Thodal, C. E., Schladow, S.G., (2009). Environmental temperature sensing using Raman spectra DTS fiber-optic methods, Water Resources Research, 45.

Varhola, A., and N. C. Coops (2013). Estimation of watershed-level distributed forest structure metrics relevant to hydrologic modeling using LiDAR and Landsat, Journal of Hydrology, 487, 70-86.

Webster, C., N. Rutter, and T. Jonas (2017). Improving representation of canopy temperatures for modeling subcanopy incoming longwave radiation to the snow surface, Journal of Geophysical Research-Atmospheres, 122(17), 9154-9172.

Webster, C., N. Rutter, F. Zahner, and T. Jonas (2016a). Measurement of Incoming Radiation below Forest Canopies: A Comparison of Different Radiometer Configurations, Journal of Hydrometeorology, 17(3), 853-864.

Webster, C., N. Rutter, F. Zahner, and T. Jonas (2016b). Modeling subcanopy incoming longwave radiation to seasonal snow using air and tree trunk temperatures, Journal of Geophysical Research-Atmospheres, 121(3), 1220-1235.

Westerling A.L., Hidalgo H.G., Cayan D.R., Swetnam T.W. (2006). Warming and earlier spring increase Western U.S. forest wildfire activity, Science, 313 (5789), 940-943.

Xia, Y. L., K. Mitchell, M. Ek, J. Sheffield, B. Cosgrove, E. Wood, L. Luo, C. Alonge, H. Wei, J. Meng, B. Livneh, D. Lettenmaier, V. Koren, Q. Duan, K. Mo, Y. Fan, D. Mocko. (2012). Continental-scale water and energy flux analysis and validation for the North American Land Data Assimilation System project phase 2 (NLDAS-2): 1. Intercomparison and application of model products, Journal of Geophysical Research-Atmospheres, 117, 27.